

# The origin of the diffuse non-thermal X-ray and radio emission in the Ophiuchus cluster of galaxies

M.A. Pérez-Torres<sup>1\*</sup>, F. Zandanel<sup>1</sup>, M.A. Guerrero<sup>1</sup>, S. Pal<sup>2</sup>, S. Profumo<sup>3</sup>, F. Prada<sup>1,4</sup>, F. Panessa<sup>5</sup>

<sup>1</sup>*Instituto de Astrofísica de Andalucía, CSIC, Apdo. Correos 3004, E-18080 Granada, Spain*

<sup>2</sup>*National Centre for Radio Astrophysics, Tata Institute of Fundamental Research, Pune, 411007, India*

<sup>3</sup>*Santa Cruz Institute for Particle Physics (SCIPP) and Department of Physics, University of California, Santa Cruz CA 95064, USA*

<sup>4</sup>*Visiting research physicist at the Santa Cruz Institute for Particle Physics (SCIPP), University of California, Santa Cruz CA 95064, USA*

<sup>5</sup>*Istituto di Astrofisica Spaziale e Fisica Cosmica (INAF), 00133 Roma, Italy*

Accepted 2009 April 7. Received 2009 April 7; in original form 2008 December 17

## ABSTRACT

We present high resolution 240 and 607 MHz GMRT radio observations, complemented with 74 MHz archival VLA radio observations of the Ophiuchus cluster of galaxies, whose radio mini-halo has been recently detected at 1400 MHz. We also present archival *Chandra* and *XMM-Newton* data of the Ophiuchus cluster. Our observations do not show significant radio emission from the mini-halo, hence we present upper limits to the integrated, diffuse non-thermal radio emission of the core of the Ophiuchus cluster. The *XMM-Newton* observations can be well explained by a two-temperature thermal model with temperatures of  $\simeq 1.8$  keV and  $\simeq 9.0$  keV, respectively, which confirms previous results that suggest that the innermost central region of the Ophiuchus cluster is a cooling core. This result is consistent with the occurrence of a mini-halo, as expected to be found in hot clusters with cool cores. We also used the *XMM-Newton* data to set up an upper limit to the (non-thermal) X-ray emission from the cluster. We also emphasize that the non-thermal X-ray emission obtained with *XMM-Newton* and *INTEGRAL* cannot be produced by the putative AGN of the galaxy at the cluster center.

The combination of available radio and X-ray data has strong implications for the currently proposed models of the spectral energy distribution (SED) from the Ophiuchus cluster. In particular, a synchrotron+IC model is in agreement with the currently available data, if the average magnetic field is in the range  $(0.02-0.3)\mu\text{G}$ . A pure WIMP annihilation scenario can in principle reproduce both radio and X-ray emission, but at the expense of postulating very large boost factors from dark matter substructures, jointly with extremely low values of the average magnetic field. Finally, a scenario where synchrotron and inverse Compton emission arise from PeV electron-positron pairs (via interactions with the CMB), can be ruled out, as it predicts a non-thermal soft X-ray emission that largely exceeds the thermal Bremsstrahlung measured by *INTEGRAL*.

**Key words:** galaxies: Galaxies: clusters: individual: Ophiuchus Cluster - Radio: galaxies: clusters - X-rays: galaxies: clusters

## 1 INTRODUCTION

Clusters of galaxies are the largest bound structures of the Universe and, according to hierarchical scenarios of structure formation, the latest ones to form. They are filled by a hot ( $10^7 - 10^8$  K) plasma, called intra-cluster medium

(ICM), and thus radiate in soft X-ray bands through thermal Bremsstrahlung. In hierarchical cosmological scenarios, the most massive clusters form as a result of merging of smaller clusters. The current scenario predict that a fraction of the energy dissipated during the merging is channeled into particles acceleration via shocks and turbulence (e.g. Sarazin 1999a; Blasi, Gabici & Brunetti 2007). This lead to a complex population of primary protons and elec-

\* E-mail: torres@iaa.es

trons in the ICM. Models predict that a large population of *secondary electrons* could be injected by collisions between relativistic and thermal protons in the ICM. Alternatively, the ICM relativistic electrons population could be *re-accelerated in situ* by various mechanisms associated with turbulence in massive merger events. The recent observation of a radio halo with a very steep synchrotron spectrum in Abell 521 by Brunetti et al. (2008) supports the turbulence acceleration mechanism. This electron population is expected to be responsible for both the synchrotron radio emission and the hard X-ray emission. The origin of the latter emission is disputed. It has been proposed that it is due to inverse-Compton (IC) scattering of relativistic electrons with the cosmic microwave background (CMB) (Atoyan & Völk 2000, Ensslin & Biermann 1998, Sarazin 1999b), or to a population of PeV electrons that would radiate in hard X-rays through synchrotron emission (Timokhin, Aharonian & Neronov 2004, Inoue, Aharonian & Sugiyama 2005). Those latter models have the disadvantage that do not explain the well-known synchrotron radio emission.

Extended radio emission in clusters of galaxies has been known to exist for a long time (see e.g. Feretti & Giovannini 2007). However, the detection of the putative hard X-ray emission has been rather elusive, apart from some rather weak and controversial detections of a hard tail in the X-ray spectrum of Coma (Fusco-Femiano et al. 2004) and Abell 2256 (Fusco-Femiano et al. 2005) with *BeppoSAX*, and the *Chandra* observations of the Perseus cluster (Sanders et al. 2004, Sanders, Fabian & Dunn 2005). Nevertheless, *INTEGRAL* failed to find an X-ray non-thermal component in the Coma cluster (Renaud et al. 2006), and recent *XMM-Newton* observations of Perseus (Molendi & Gastaldello 2008) did not confirm Sanders et al. (2004) and Sanders, Fabian & Dunn (2005) results.

The Ophiuchus cluster is a nearby ( $z=0.028$ , Johnston et al. 1981) rich cluster located above the direction of the Galactic Center ( $l = 0.5^\circ$ ,  $b = 9.4^\circ$ ), with a very high plasma temperature ( $kT \sim 10$  keV). Johnston et al. (1981) claimed, based on radio data available at the time, that the cluster was associated with the steep-spectrum radio source MSH 17-203 (also dubbed Cul 1709-231). The identification of this radio source as a radio halo from the Ophiuchus cluster would thus imply the presence of relativistic electrons, and hence the presence of a non-thermal, high-energy tail in the X-ray band would be expected. And, in fact, while this paper was being refereed, Govoni et al. (2009) and Murgia et al. (2009) have reported the detection of a radio mini-halo in the Ophiuchus cluster (see Fig. 6 in Govoni et al. 2009), using deep VLA 1400 MHz observations.

Watanabe et al. (2001), based on *ASCA* data, found that the core of the cluster has an angular diameter of  $6.4'$ . Measurements of the ICM temperature vary from  $8.5 \pm 0.5$  keV (*INTEGRAL*; Eckert et al. 2008) up to  $9.5^{+1.4}_{-1.1}$  keV (Swift/BAT; Ajello et al. 2008). Watanabe et al. also found a large ( $20' \times 30'$ ), hot ( $kT > 13$  keV) region,  $20'$  west of the cluster center, from which they concluded that the cluster is not dynamically relaxed, and suggested it experienced a major merging event in the recent past ( $t \lesssim 1$  Gyr). Eckert et al. (2008) have recently reported a tentatively resolved ( $\sim 5'$ ) X-ray source at the cluster center, and claimed the presence of a non-thermal tail. Eckert et al. interpret the non-thermal hard X-ray emission as due

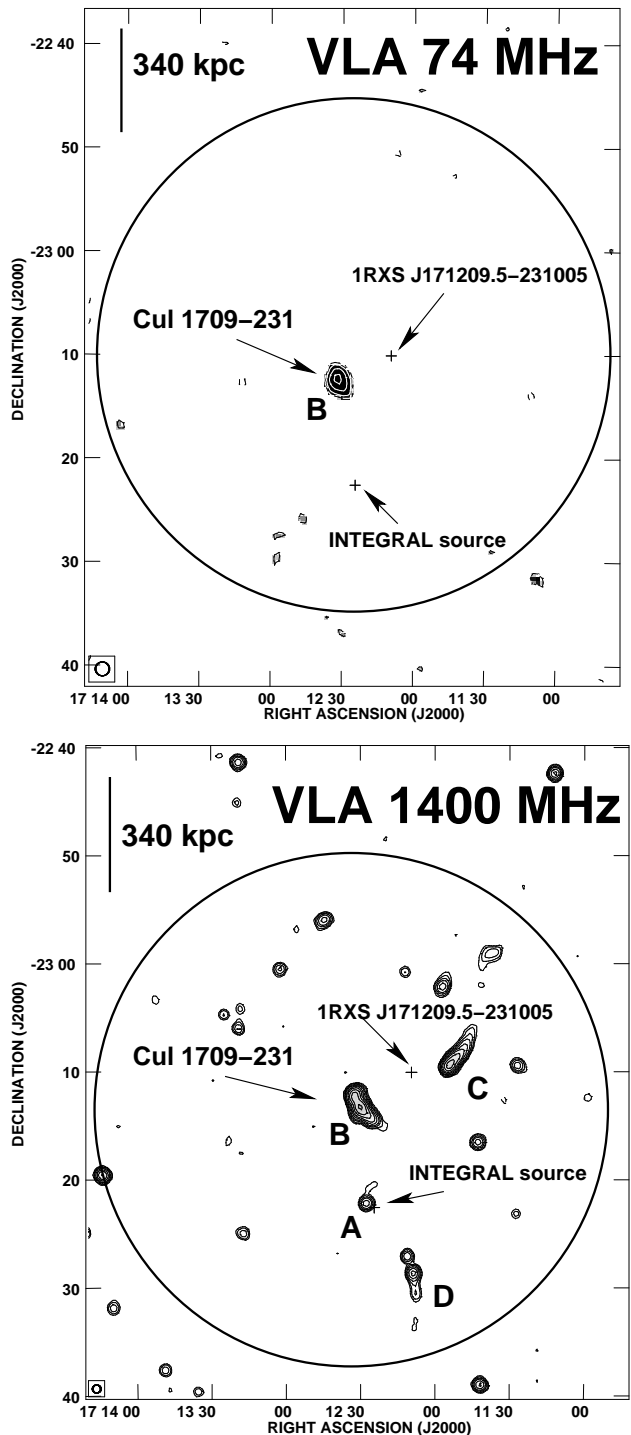


**Figure 1.** VLSS radio image at 74 MHz (top) and NVSS radio image at 1400 MHz (bottom) of the Ophiuchus Cluster. In both panels the positions of the *INTEGRAL* X-ray detection and of the nearest X-ray source 1RXS J171209.5-231005 are shown. The synthesized beams (FWHM) at 74 MHz and 1400 MHz were ( $80'' \times 80''$ ) and ( $45'' \times 45''$ ), respectively, and are drawn at the bottom left of each panel. The big circles in the panels correspond to the approximate size of the synthesized beam of the FLEURS and SYDNEY (big circle in top panel) and of the OSU (big circle in the bottom panel) radio observations (see Table 1), carried out in the 70's. Note that the radio emission of a large amount of different sources enters the beam, and therefore heavily overestimates the flux at those frequencies. The off-source rms noise in the VLSS and NVSS images is of 220 mJy/b and 0.4 mJy/b.

to IC radiation from relativistic electrons scattered off the CMB in the cluster medium. The evidence of a non-thermal hard X-ray tail in the Ophiuchus cluster from *INTEGRAL* could be the first significant detection of such non-thermal X-ray emission from a galaxy cluster. More recent Suzaku observations of the Ophiuchus cluster by Fujita et al. (2008) have, however, failed to detect the non-thermal component claimed by Eckert et al. (2008), although their quoted upper limit of  $2.8 \times 10^{-11}$  erg cm $^{-2}$  s $^{-1}$  in the 20 – 60 keV energy band is still compatible with the *INTEGRAL* detection. Fujita et al. (2008) found that the cluster was hot, except for the innermost  $\sim 50$  kpc, and that the intra-cluster medium (ICM) was in ionization equilibrium state. From those results, Fujita et al. conclude that Ophiuchus cluster is not a major merger, but one of the hottest clusters with a cool core.

Even more recently, Ajello et al. (2008) have found, combining Swift/BAT and *Chandra* spectra, an upper limit on the Ophiuchus non-thermal X-ray emission in the 20 – 60 keV band, of  $7.2 \times 10^{-12}$  erg cm $^{-2}$  s $^{-1}$ , which is below the *INTEGRAL* detection. Nevertheless, the claimed *INTEGRAL* detection, the Suzaku and the combined Swift/BAT and *Chandra* upper limits are consistent.

In this Paper, we present and discuss archival and new radio data for the Ophiuchus cluster, along with archival X-ray data. Together with the published X-ray data of the cluster, we model all the data to shed light on the origin of the diffuse non-thermal emission from this cluster of galaxies. In Section 2, we present the VLA and GMRT radio data from the Ophiuchus cluster, along with archival *Chandra* and *XMM-Newton* data. In Section 3, we model the SED of the Ophiuchus cluster using several different scenarios. Finally, we summarize our main results and their implications in Section 4. All sky positions in the paper are for the J2000.0 equinox. We assume cosmological parameters of  $\Omega_0 = 0.3$ ,  $\lambda_0 = 0.7$  and  $H_0 = 70$  km s $^{-1}$  Mpc $^{-1}$ . For these parameters, our assumed redshift of 0.028 to the Ophiuchus cluster (Johnston et al. 1981) corresponds to a luminosity distance of 122.6 Mpc and a comoving distance of 126.03 Mpc. At this distance, 1'' corresponds to 560 pc.

## 2 OBSERVATIONS AND RESULTS

We present in Table 1 a summary of all the relevant data for the Ophiuchus cluster, spanning 11 decades of energy from the radio up to gamma-rays, and which include both data from the literature and obtained by us (this paper). We present the main results of these observations in Figures 1 through 4, where we show high-resolution radio and X-ray images of the Ophiuchus cluster of galaxies.

### 2.1 Radio observations

#### 2.1.1 Data from the literature

The first five rows of Table 1 show the radio measurements of the Ophiuchus cluster of galaxies, compiled by Johnston et al. (1981), and have been used in the past to model the SED from the Ophiuchus cluster (e.g., Eckert et al. 2008, Proffo et al. 2008). We note that these rather old radio data

have significantly poorer resolution than is currently available with existing radio interferometer arrays, and therefore the use of higher resolution radio data might have a relevant impact on the modelling of the spectral energy distribution (SED) of the Ophiuchus cluster. In particular, the old radio data at 30, 86 and 1400 MHz cover a too large area of sky (see the drawn circles in Figure 1), so that the radio emission of a large amount of different sources enters into the beam, and therefore heavily overestimates the flux at those frequencies.

#### 2.1.2 VLA data

Fig. 1 shows publicly archival Very Large Array (VLA) radio images of the Ophiuchus Cluster at 74 MHz (top), taken as part of the VLA Low-frequency Sky Survey (VLSS; Cohen et al. 2007), and at 1400 MHz (bottom; NRAO VLA Sky Survey - NVSS; Condon et al. 1998). Note that the two Culgora data measurements at 80 and 160 MHz in Table 1 were obtained with resolutions of a few arcmin. The dominant radio source appears to be Cul 1709-231 (RA=17<sup>h</sup>12<sup>m</sup>29.70<sup>s</sup>, DEC=-23°12'6"). This source position coincides within the errors with the only radio source that is clearly detected at 74 MHz in the VLSS image (upper panel of Figure 1), which has a resolution of 80". The emission peak ( $\approx 4.2$  Jy/beam) does indeed correspond to the source Cul 1709-231, for which we obtain RA=17<sup>h</sup>12<sup>m</sup>31.30<sup>s</sup> and DEC=-23°12'24.26", with a positional uncertainty of 2.6" in each coordinate. In the 74 MHz VLSS image (top panel of Figure 1), Cul 1709-231 is extended, and has a total flux of  $\sim 8.0$  Jy. However, its position is  $\sim 17'$  off the maximum of emission obtained with *INTEGRAL* by Eckert et al. (2008). (We used Fig. 1 in Eckert et al. to determine the position of the maximum of emission of the *INTEGRAL* source: RA=17<sup>h</sup>12<sup>m</sup>24.50<sup>s</sup>, DEC=-23°22'35.0", with an estimated uncertainty of  $\approx 1.8'$  in each coordinate). Since the core radius is 3.2' (Watanabe et al. 2001, Eckert et al. 2008), it is unlikely that Cul 1709-231 can be physically related with the core of the cluster. In fact, the very recent discovery of the radio mini-halo close to source A shows that Cul 1709-231 is not related at all with the cluster core.

The archival 1400 MHz NVSS image (bottom panel of Figure 1) has two times better resolution than the 74 MHz image, and shows a considerably larger number of radio sources. This comes as no surprise, since the off-source rms in the VLSS image of the Ophiuchus region is 220 mJy/b, while that of the NVSS image is  $\approx 0.4$  mJy/b, i.e., the NVSS image is 550 times more sensitive, and therefore is able to detect many sources that went undetected in the VLSS image. In particular, we found a relatively faint ( $S_\nu \approx 50$  mJy) radio source (dubbed A in the bottom panel of Fig. 1) at RA=17<sup>h</sup>12<sup>m</sup>27.47<sup>s</sup>, DEC=-23°22'04.9". This position is  $\sim 6''$  away from the optical position of an elliptical, cD galaxy at  $z = 0.028456$  (2MASX J17122774-2322108), which may suggest that the radio emission arises from it (see also sections 2.1.3, 2.2 and Figure 3). The off-source rms around this source is of about 1.0 mJy/b.

Very recently, Govoni et al. (2009) and Murgia et al. (2009) have detected a (radio) mini-halo in the Ophiuchus cluster (see Fig. 6 in Govoni et al. 2009), using deep VLA 1400 MHz observations. Murgia et al. (2009) report a flux density of  $\approx 106$  mJy for this mini-halo, and a size of  $\approx 9 \times 12$

arcmin<sup>2</sup>. It is also not surprising that the NVSS archival image did not show evidence for the mini-halo, since the off-source rms attained by Govoni et al. (2009) was of 0.1 mJy/b, five times deeper than the overall off-source rms in the NVSS image we used (and ten times deeper than the off-source rms around the radio emission detected from the cD galaxy - see previous paragraph - which is the relevant figure). Thus, while both our archival NVSS image and that of Govoni et al. clearly detect the central, compact emitting source, the much poorer sensitivity of the public NVSS image prevented us from detecting the mini-radio halo at 1400 MHz.

### 2.1.3 GMRT radio observations

We observed the field of the Ophiuchus Cluster on 23 May 2008 for about two hours, using the Giant Metrewave Radio Telescope (GMRT) near Pune, India. The GMRT is an array of thirty fully steerable, parabolic radio antennas of 45 meter diameter each, spread over an area of 25 km in size. 16 of the antennas are displayed along three arms, with nearly a ‘Y’ shape, and the remaining 14 antennas are placed within one kilometer of the central part of the array. We observed simultaneously at the sky frequencies of 240 and 607 MHz, using synthesized bandwidths of 6 and 32 MHz, respectively. We observed in spectral line mode, with channels widths of 125 KHz, to be able to accurately remove the radio frequency interference (RFI), which affects heavily low-frequency radio observations. We used 3C 286 as flux and band-pass calibrator, and used Baars et al. (1977) to set the flux density scale, and used B1822-096 as phase calibrator. We edited, flagged, and calibrated the data within the NRAO Astronomical Imaging Processing Software (*AIPS*). After these calibration steps, we averaged our data to increase the signal to noise ratio, resulting in effective channel widths of 1 and 2 MHz at 240 and 607 MHz, respectively. Because of the small bandwidth, sources in our fields are not affected by bandwidth smearing problems. We then imaged and self-calibrated the data (see Fig. 2) also within *AIPS*, and corrected the images for their beamshape, yielding final resolutions of  $25.8'' \times 13.5''$  and  $7.1'' \times 6.1''$  at 240 and 607 MHz, respectively.

### 2.1.4 Sources in the field of the Ophiuchus cluster and upper limits to its diffuse radio emission

We performed an extensive search for positional coincidences of the local maxima in our 607 MHz GMRT image, using the NASA Extragalactic Database (NED), aimed at confirming (or ruling out) the physical belonging of the radio sources to the Ophiuchus cluster of galaxies. The search for counterparts was performed within a 3' radius from the given positions and we summarize our results in Table 2. The position of the radio and X-ray peak (*Chandra*, see section 2.2) of source A lies very close to the position of 2MASX J1722774-2322108 (Hasegawa et al. 2000), an elliptical cD galaxy at  $z=0.028$ , and which is at the center of the Ophiuchus cluster. Source B coincides with source Cul 1709-231 and with NVSS J171224-231424, which is approximately located at 1.5' in the SE direction from the local maximum of radio emission. NED classifies those sources simply as radio sources where Cul 1709-231 is described as extended;

no redshift measurements are available for those sources. The source C coincides with the source 2MASX J17115542-239423, an elliptical galaxy with redshift  $z = 0.027$ , and with PMN J1711-2308, located at  $\sim 1'$  in the NE direction, from the source local maximum and it is classified as a radio source with no redshift measurement available. Source D-north perfectly coincides with NVSS J171211-232705, a radio source with no redshift measurement available. Finally, the source D-south position matches extremely well with the position of 2MASX J17120908-2328263, an elliptical galaxy with redshift  $z = 0.025$ , and with the source NVSS J171208-232839, classified as a radio source and with no redshift measurement available.

We therefore consider that source A is at the center of the Ophiuchus cluster, and suggest that sources C and D-south are very likely members of the Ophiuchus cluster, given their redshift. Visual inspection of archival NED optical images reveals that PMN J171224-231424 and NVSS J171211-232705 are probably galaxies. However, spectroscopic follow-up is needed in order to determinate their redshift and confirm their cluster membership. This is very important above all for the Cul 1709-231, NVSS J171224-231424 and NVSS J171208-232839 sources, for which the image inspection reveals no clear evidence for optical counterparts. In particular, the Culgora source characterization is very important in order to establish its properties and cluster membership, given that, in the past, it was confused with the central elliptical cD galaxy (source A) due to the poor resolution of the old radio data (Johnston et al. 1981).

We also used our 240 and 607 MHz GMRT images (see Fig. 2), along with the archival 74 VLA image (see Fig. 1), to obtain upper limits to the diffuse, non-thermal radio emission from the Ophiuchus cluster of galaxies. In particular, we used an area of  $\approx 9 \times 12$  arcmin<sup>2</sup>, very similar to the size of the radio mini-halo found by Govoni et al. (2009), and centered in source A (the core of the cluster). We then excised the flux density of this point-like source in our images, and present upper limits to those measurements in Table 1. These were obtained by multiplying the angular area above (after being converted into a number of beams at each frequency), by the off-source rms 74, 240, and 607 MHz (220, 5, and 0.4 mJy/b, respectively). From the upper limits at low frequencies, and the detection of the Ophiuchus cluster (mini-halo) at 1400 MHz, we obtain an upper limit to the (radio) spectral index of  $\beta \lesssim 1.73$  ( $S_\nu \propto \nu^\beta$ ). If we adopt a  $3\sigma$  upper limit to the non-detected extended radio emission, this yields an upper limit for the spectral index of  $\beta \lesssim 2.09$ . Those values are consistent with typical radio spectral indices found in radio mini-halos ( $\beta \gtrsim 1.5$ ; Ferrari et al. 2008).

## 2.2 X-ray observations

The *Chandra* X-ray Observatory observed the Ophiuchus cluster for 51.2 ks (obs. ID 3200) on 2002 October 21. The Advanced CCD Imaging Spectrometer (ACIS) instrument was used and the core of the cluster was imaged on the back-illuminated CCD S3. The data were processed using the standard data processing version DS 7.6.9 and subsequently analyzed using the *Chandra* Interactive Analysis of Observations (CIAO) software package version 4.0. The observations were not affected by any period of high-background, and no

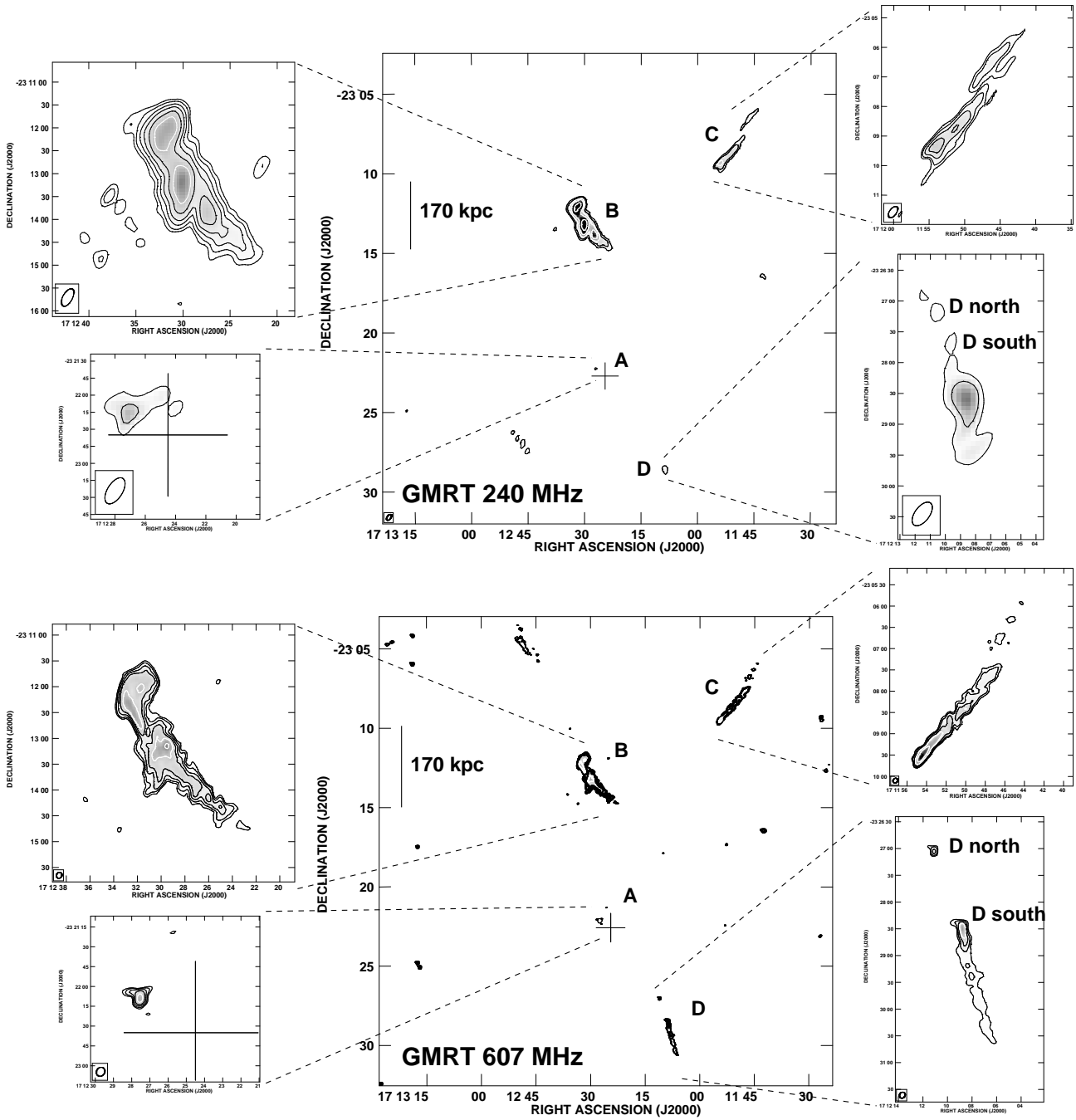


**Figure 2.** GMRT images at 240 MHz (top) and 607 MHz (bottom) of the Ophiuchus Cluster region. In both panels, the cross marks the position of the *INTEGRAL* X-ray detection. The synthesized beams (FWHM) at 240 MHz and 607 MHz were  $26.1'' \times 13.5''$  and  $7.1'' \times 6.1''$ , respectively, and are drawn in the bottom left part of each panel (the linear size shown in the images have been calculated for an assumed redshift of  $z = 0.028$ ). The off-source rms noise of the 240 and 607 MHz images is of 5.0 mJy/b and 0.4 mJy/b, respectively. Contours are drawn starting at three times the quoted rms, and increase in steps of  $\sqrt{3}$ .

time intervals had to be excised. The final exposure time was 50.5 ks.

*XMM-Newton* also observed the Ophiuchus cluster for 36.7 ks (obs. ID 0505150101) during revolution 1416 on 2007 September 2. The European Photon Imaging Camera (EPIC) pn was used in the extended full frame mode for 26.8 ks with the medium filter. The data were processed starting from the odv files with the *XMM-Newton* SAS software

(version 7.1.2). X-ray events corresponding to patterns 0-4 were selected. Exposure has been filtered for periods of high background with an effective exposure of 20 ks. *Chandra* and *XMM-Newton* spectra have been analyzed using HEASARC XSPEC v11.0.1 routines (Arnaud 1996).

We have used the *Chandra* observations of the Ophiuchus cluster to obtain a high-resolution X-ray image of its central region (Figure 3-top). The *Chandra* observations are

**Table 1.** Summary of the available radio, X and gamma-ray non-thermal measurements of the Ophiuchus cluster.

Instruments	$\nu$ [MHz]	E [eV]	FWHM [']	F [Jy]	EF [erg cm <sup>-2</sup> s <sup>-1</sup> ]	References
FLEURS	29.9	$1.24 \times 10^{-7}$	48×48	215 ± 16	$(6.43 \pm 0.48) \times 10^{-14}$	[1]
CULGORA	80	$3.31 \times 10^{-7}$	3.7×3.7	23 ± 2	$(1.84 \pm 0.16) \times 10^{-14}$	[1]
SYDNEY	86	$3.56 \times 10^{-7}$	50×50	42 ± 4	$(3.61 \pm 0.34) \times 10^{-14}$	[1]
CULGORA	160	$6.62 \times 10^{-7}$	1.9×1.9	6.4 ± 0.1	$(1.02 \pm 0.02) \times 10^{-14}$	[1]
OSU	1415	$5.85 \times 10^{-6}$	40×40	0.8 ± 0.2	$(1.13 \pm 0.28) \times 10^{-14}$	[1]
VLA	74	$3.06 \times 10^{-7}$	1.33×1.33	< 13.43	< $9.89 \times 10^{-15}$	This work
GMRT	240	$9.93 \times 10^{-7}$	0.44×0.23	< 5.34	< $1.32 \times 10^{-14}$	This work
GMRT	607	$2.51 \times 10^{-6}$	0.12×0.10	< 3.60	< $2.24 \times 10^{-14}$	This work
VLA	1400	$5.79 \times 10^{-6}$	1.52×0.67	0.106 ± 0.030	$(1.48 \pm 0.42) \times 10^{-15}$	[2]
XMM-Newton (EPIC)	$1.2 - 24.2 \times 10^{11}$	$0.3 - 9 \times 10^3$	0.1	$\lesssim 1.14$	$\lesssim 1.44 \times 10^{-11}$	This work
SUZAKU (90% UL)	$0.5 - 1.5 \times 10^{13}$	$2 - 6 \times 10^4$	2	< $2.9 \times 10^{-7}$	< $2.8 \times 10^{-11}$	[3]
Swift/BAT (90% UL)	$0.5 - 1.5 \times 10^{13}$	$2 - 6 \times 10^4$	20	< $7.6 \times 10^{-8}$	< $7.2 \times 10^{-12}$	[4]
INTEGRAL (IBIS/ISGRI)	$1.21 \times 10^{13}$	$(4 - 6) \times 10^4$	12	$(7.93 \pm 1.32) \times 10^{-8}$	$(9.61 \pm 1.61) \times 10^{-12}$	[5]
INTEGRAL (IBIS/ISGRI)	$1.69 \times 10^{13}$	$(6 - 8) \times 10^4$	12	$(4.97 \pm 2.66) \times 10^{-8}$	$(8.41 \pm 4.49) \times 10^{-12}$	[5]
EGRET (2 $\sigma$ UL)	$2.4 \times 10^{17} - 10^{19}$	$10^8 - 10^{10}$	(6-30)	< $3.8 \times 10^{-13}$	< $9.1 \times 10^{-12}$	[6]

Note that the two CULGORA flux density values correspond to measurements of the cluster Source B, since its resolution was good enough. On the contrary, the FLEURS, SYDNEY and OSU had poorer resolutions, thus covering a too large area of sky (see Figure 1 and text for details), and therefore including the radio emission from multiple sources in the field.

References: [1] Johnston et al. (1981), [2] Murgia et al. (2009), [3] Fujita et al. (2008), [3] Ajello et al. (2008), [5] Eckert et al. (2008), [6] Reimer et al. (2003).

**Table 2.** List of the sources found in the GMRT images field of view with the corresponding NED coincident sources.

Source	$\nu$ [MHz]	RA	DEC	Peak [mJy/beam]	Total Flux [mJy]	Coincidence	$z$	Type
A	607 240	17 <sup>h</sup> 12 <sup>m</sup> 27.56 <sup>s</sup>	-23°22'09.5''	29.1 33	37.8 ± 1.0 38 ± 5	2MASX J17122774-2322108	0.028	G-cD
B	607 240	17 <sup>h</sup> 12 <sup>m</sup> 29.51 <sup>s</sup>	-23°13'09.4''	38.7 391	2020 ± 21 4853 ± 30	Cul 1709-231 NVSS J171224-231424	- -	R-S R-S
C	607 240	17 <sup>h</sup> 11 <sup>m</sup> 54.52 <sup>s</sup>	-23°09'32.8''	31.3 102	579 ± 7 1117 ± 7	2MASX J17115542-2309423 PMN J1711-2308	0.027 -	G-E R-S
D (north)	607 240	17 <sup>h</sup> 12 <sup>m</sup> 11.10 <sup>s</sup>	-23°27'03.9''	8.9 17	11.2 ± 0.8 83 ± 5	NVSS J171211-232705	-	R-S
D (south)	607 240	17 <sup>h</sup> 12 <sup>m</sup> 08.769 <sup>s</sup>	-23°28'29.62''	20 44	161 ± 2 263 ± 5	2MASX J17120908-2328263 NVSS J171208-232839	0.025 -	G-E R-S

Source positions (J2000.0) corresponding to the local maxima of our 607 MHz GMRT image. The type, classification, and redshift  $z$  for the sources are obtained from NED (Type: G-cD, G-E and R-S stand for elliptical cD galaxy, elliptical galaxy and radio source, respectively).

especially suited for the study of point-like sources, while the extended, diffuse emission of this cluster is difficult to study because its spatial extension is much larger than *Chandra* ACIS field of view. Therefore, we did not use the *Chandra* measurements to estimate a limit to the diffuse X-ray emission of the cluster, and hence this information is not included

in Table 1. The analysis of the brightness radial profile of the central region shows the presence of a relatively bright point-like source at the core of the Ophiuchus cluster with position RA=17<sup>h</sup>12<sup>m</sup>27.64<sup>s</sup>, DEC=-23°22'07".5 (the uncertainty in each coordinate is  $\approx 1''$ ). The central source profile is clearly point-like. and cannot be modeled by classical cluster pro-

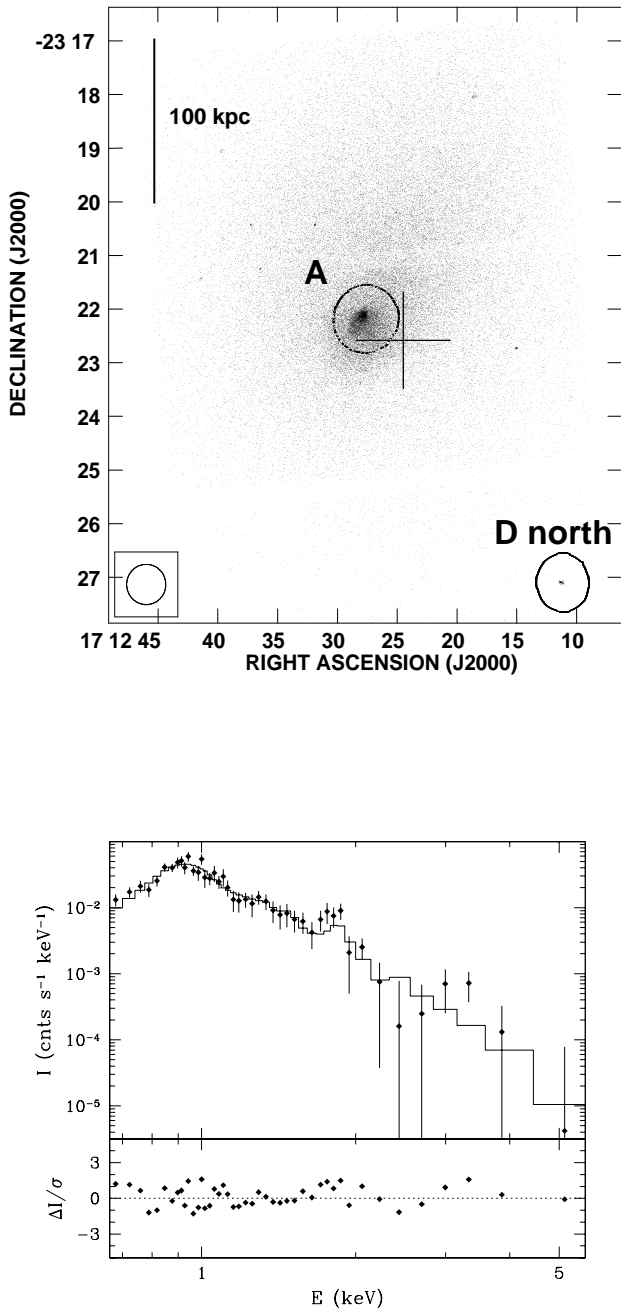


**Figure 3.** (*Top*) *Chandra* ACIS greyscale image of the core of the Ophiuchus cluster overplotted with  $10\sigma$  NVSS 1400 MHz radio contours. The locations of sources A and D north, coincident with two point-like X-ray sources, are labeled on the plot. The cross marks the position of the *INTEGRAL* source detected by Eckert et al. (2008). (*Bottom*) Background-subtracted *Chandra* ACIS spectrum of the point source at the core of the Ophiuchus cluster overplotted with the best-fit MEKAL model. The residuals of the best-fit model are shown in the lower panel.

file models (such as King, Beta-models, etc.). The location of this point source is only  $3.5''$  away from the elliptical cD galaxy 2MASX J17122774-2322108. Furthermore, Fig. 3-*top* shows that the NVSS 1400 MHz radio peak of the radio emitting source A matches well with the location of the X-ray point source at the core of the Ophiuchus cluster. This spatial coincidence suggests that the radio emission from source A and the X-ray emission from the point source at the core of the Ophiuchus cluster are associated. The radio emission from source A (see Table 2) indicates a flat spectrum, which suggests that its radio emission is AGN-like, and thus the nuclear activity of the cD galaxy 2MASX J17122774-2322108 can be claimed responsible for the radio and X-ray emission.

The *Chandra* ACIS X-ray spectrum of the point source at the core of the Ophiuchus cluster was extracted using CIAO from a circular region of radius  $2''$  centered at its position. The background-subtracted X-ray spectrum presented in the lower panel of Fig. 3 shows a bright peak at  $\sim 0.9$  keV, and relatively fainter peaks at  $\sim 1.5$  and  $\sim 1.8$  keV. This spectral shape suggests the presence of line emissions as can be expected from an optically-thin emitting plasma. Indeed, the spectrum is well fitted using a single temperature MEKAL model with plasma abundances  $0.3 Z_{\odot}$  adequate for the central regions of the Ophiuchus cluster (Watanabe et al. 2001), with a temperature  $kT$  of 0.78 keV, and a column density of  $4.2 \times 10^{21} \text{ cm}^{-2}$ . The quality of the fit suggests that a non-thermal X-ray contribution is negligible. The unabsorbed flux in the 0.3 to 9.0 keV energy band is  $F \approx 1.9 \times 10^{-13} \text{ erg cm}^{-2} \text{ s}^{-1}$ . At the distance of the Ophiuchus cluster, this implies an intrinsic luminosity  $L_X \approx 3.3 \times 10^{41} \text{ erg s}^{-1}$ . The absence of a non-thermal X-ray component suggests that the central nucleus is very weak and/or highly absorbed. Even if the *Chandra* X-ray luminosity is entirely associated with the central active nucleus, this must be of low luminosity. Indeed, no recent strong AGN activity has been observed at the cluster center (Dunn & Fabian 2006). Therefore, the activity of the nucleus of this galaxy cannot be claimed responsible of the hard X-ray emission detected by *INTEGRAL*.

The *XMM-Newton* EPIC-pn observations have been used to investigate the X-ray emission from the core of the Ophiuchus cluster given its sensitivity to low surface brightness diffuse X-ray emission. In order to assess the occurrence of non-thermal emission from the mini-halo at the core of the Ophiuchus cluster, a spectrum has been extracted from a circular region of radius  $5''$  centered at the position of the cluster core that encompasses the radio mini-halo region (Govoni, priv. comm.). The corresponding background spectrum has been obtained from a  $50''$  radius region off-set  $\sim 10'$  from the cluster core in the same CCD<sup>1</sup>. The most up-

<sup>1</sup> For comparison, we also considered two different background spectra: one extracted from the same observations from a distant circular region in EPIC-pn CCD 12 off-set  $\sim 14.5'$  from the cluster core, and another one built composed of the sky background given by the *ROSAT All Sky Survey* (RASS) and the particle background given by the *XMM-Newton* closed filter data, kindly provided by J. H. Nevalainen. No significant differences were found in the background subtracted spectrum of the core of the Ophiuchus cluster using these three different background spectra, basically because the cluster brightness is  $\gtrsim 100$  times brighter than the background emission.

dated calibration files available at the time of the reduction were used to generate the ancillary and detector response matrices using the *XMM-Newton* SAS *arfgen* and *rmfgen* tasks.

The background-subtracted spectrum displayed in Figure 4 shows a bright and broad peak at  $\sim 1.08$  keV, and fainter peaks at  $\sim 1.4$  keV, and  $\sim 1.7$  keV. It is also very noticeable a hard energy tail up to 10 keV, as well as a prominent double-peaked emission line at  $\sim 6.4$  keV and  $\sim 6.7$  keV, which corresponds to Fe-K emission lines. The spectrum can be relatively well fitted ( $\chi^2/\text{DoF}=1.16$ ) by a two-temperature MEKAL model. The best-fit model has a hydrogen column density  $N_{\text{H}} = 3.2 \times 10^{21} \text{ cm}^{-2}$ , and temperatures of  $kT = 1.8 \pm 0.3$  keV and  $kT = 9.0 \pm 0.2$  keV. The total unabsorbed flux in the 0.3 to 9.0 keV energy band is  $F \approx 2.5 \times 10^{-10} \text{ erg cm}^{-2} \text{ s}^{-1}$ , corresponding only a flux of  $F \approx 4.5 \times 10^{-12} \text{ erg cm}^{-2} \text{ s}^{-1}$  to the soft component, i.e., the X-ray spectrum of this region is dominated by the hard emission associated to the outermost regions of the cluster seen in projection towards its core. This result is consistent with the conclusion obtained by Fujita et al. (2009) that Ophiuchus hosts a cool core, and yields support to their suggestion that Ophiuchus is not the result of a major merger event.

The addition of an additional power law component with an assumed photon index of  $\Gamma = 1.6$  (Eckert et al. 2007) does not improve significantly the fit ( $\chi^2/\text{DoF}=1.17$ ), and thus such a component can be discarded. The  $3\text{-}\sigma$  upper limit of the unabsorbed flux of such component has been estimated to be  $F \leq 1.44 \times 10^{-11} \text{ erg cm}^{-2} \text{ s}^{-1}$ . At the distance of the Ophiuchus cluster, this implies an upper limit to the intrinsic luminosity of non-thermal emission of  $L_X(\text{pow}) \leq 2.5 \times 10^{43} \text{ erg s}^{-1}$ .

### 3 MODELLING THE SED OF THE OPHIUCHUS CLUSTER

We have mentioned earlier in this paper that the radio flux density values used previously by others to model the SED of the core of the Ophiuchus cluster significantly overestimated the actual ones, due to the huge synthesized beams of the old radio observations (Johnston et al. 1981; see also Figure 1). Therefore, the use of those radio flux densities to constrain the properties of the Ophiuchus SED (Eckert et al. 2008) as well as to test proposed models for dark matter annihilation (Profumo 2008) should be updated according to the data presented earlier in this paper. In this section, we model and interpret the SED of the Ophiuchus cluster of galaxies, using our high-resolution, high-sensitivity measurements at 240 and 607 MHz, along with the 74 MHz VLA measurements (using archival data), the recent 1400 MHz VLA measurements of the Ophiuchus radio mini-halo (Govoni et al. 2009, Murgia et al. 2009), and the high-energy measurements quoted in Table 1. In particular, and as shown in previous sections, we obtained upper limits to the diffuse non-thermal radio emission of the cluster at low frequencies and an upper limit to luminosity of the non-thermal emission from *XMM-Newton* data (see Sect. ??).

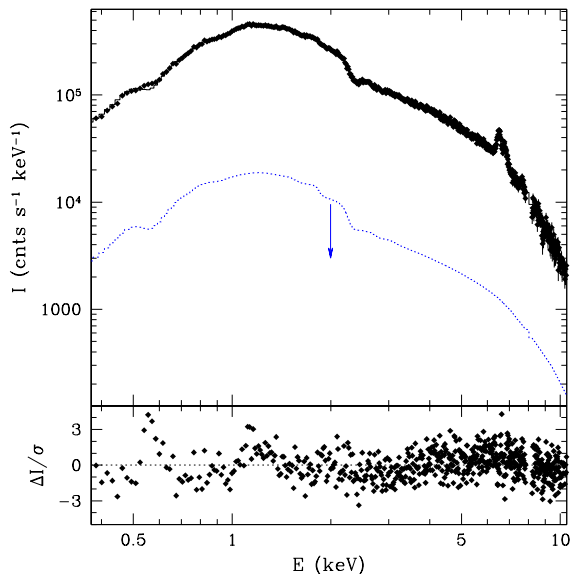


**Figure 4.** Background-subtracted *XMM-Newton* EPIC-pn spectrum of the central region of the Ophiuchus cluster overplotted with the best-fit two-temperature MEKAL model. The  $3\text{-}\sigma$  upper limit for a non-thermal component is shown as a dotted blue histogram. The residuals of the best-fit two-temperature MEKAL model are shown in the lower panel.

#### 3.1 Dark matter models

The new radio measurements permit to set stringent limits on the synchrotron radiation produced by a population of non-thermal electrons and positrons. In turn, this sets limits on weakly interacting massive particle (WIMP) dark matter models. Indeed, the pair-annihilation of WIMPs produces, as a result of the hadronization and decay of particles in the standard model, energetic electrons and positrons. The limits that can be set depend on the WIMP model (specifically, on the WIMP mass, pair-annihilation cross section and dominant annihilation final state), as well as on the dark matter density profile and on the average magnetic field in the cluster. We refer the reader to Totani (2004), Colafrancesco, Profumo & Ullio (2006), Colafrancesco, Profumo & Ullio (2007), Jeltama and Profumo (2008) and Profumo (2008), where the multi-frequency emission from WIMP annihilation has been discussed in detail. In particular, we use here the same approach as in Colafrancesco et al. (2006) and in Profumo (2008), and model the dark matter density distribution in the Ophiuchus cluster according to what described in Profumo (2008).

The new limits on the radio emission are compatible, in principle, with the WIMP annihilation interpretation of the hard X-ray flux from Ophiuchus presented in Profumo (2008). However, the magnetic field required to be consistent with our new measurements is extremely low, of the order of  $10^{-2}$  to  $10^{-3} \mu\text{G}$ .

Nonetheless, we can turn our radio data into limits on WIMP models. For this purpose, we make more conservative assumptions on the density profile and substructures than



those made in Profumo (2008). In particular, we assume a concentration  $c_{\text{vir}} = 10$  and a Navarro, Frenk and White profile (Navarro, Frenk & White 1996). In addition, we assume that 10% of the mass belongs to substructures, and that the average concentration bias in subhalos versus the host halo is  $\langle c_s \rangle / \langle c_{\text{vir}} \rangle \sim 2$ , which gives a weighted enhancement factor  $\Delta^2 \sim 6 \times 10^5$ , in the notation of Eq.(29-31) of Colafrancesco et al. (2006). Integrating over the line of sight the number density of dark matter particle pairs, we find that the radiation resulting from WIMP annihilations in Ophiuchus is given by:

$$\frac{d\Phi_\gamma}{dE_\gamma} = 2.4 \times 10^{-13} \left( \frac{\langle \sigma v \rangle_0}{3 \times 10^{-26} \text{ cm}^3 \text{ s}^{-1}} \right) \times \left( \frac{100 \text{ GeV}}{m_{\text{WIMP}}} \right)^2 \frac{dN_\gamma}{dE_\gamma} \text{ GeV}^{-1} \text{ cm}^{-2} \text{ s}^{-1} \quad (1)$$

where  $dN_\gamma/dE_\gamma$  indicates the flux of photons resulting from one dark matter annihilation event. Had we assumed a cored profile for the dark matter distribution, we would have obtained a flux a factor 2 smaller than indicated in the previous equation: unlike for nearby structures, the dependence on the details of the dark matter density distribution are not clearly for distant systems.

We show in the top panel of Fig. 5 the limits we obtain, at the 95% C.L., for a final state typical of neutralino dark matter in the minimal supersymmetric extension of the standard model, namely  $b\bar{b}$  (Jungman, Kamionkowski & Griest 1996, Bertone, Hooper & Silk 2005), for two values of the magnetic field. We also shade in gray the region excluded by the EGRET limit on the gamma-ray flux (integrated flux above 0.1 GeV larger than  $5 \times 10^{-8}$  ph/(cm<sup>2</sup> s), Reimer et al. 2003), and the line corresponding to the sensitivity of the Large Area Telescope (LAT) on-board the Fermi Gamma-Ray Space Telescope (formerly known as GLAST) sensitivity in one year of operations. For the latter, we assume a sensitivity of  $2 \times 10^{-10}$  ph/(cm<sup>2</sup> s) above 1 GeV<sup>2</sup>. The green band shows the range of values for the pair annihilation cross section typically associated with thermal dark matter production in the early universe (Jungman, Kamionkowski & Griest 1996, Bertone, Hooper & Silk 2005). The bottom panel indicates the limits we get for Kaluza-Klein WIMP dark matter in the context of Universal Extra-Dimensions (Hooper & Profumo 2007). The green line shows the typical value for the cross section expected in those models (specifically in the minimal setup). We notice that with a magnetic field of the order of 1  $\mu\text{G}$ , we are able to place rather stringent limits on dark matter models. The precise limits, however, depend crucially on the average magnetic field. Fig. 6 illustrates that there exist models that fit both the VLA radio data point and the hard X-ray emission from Ophiuchus (blue solid line). The implied needed boost factor from dark matter substructures is however very large, and the magnetic field is very small ( $\sim 50$  nG). Large boost factors can be due to either a non-standard cosmological setup or a dark matter production mechanism in the early universe, or to a more extreme substructure setup than what employed in Profumo (2008), or to a combination of both

effects. Clearly, for reasonable values of the magnetic field, radio data put the most stringent limits on dark matter annihilation in the Ophiuchus cluster. In Fig. 6, the MAGIC I and MAGIC II Imaging Atmospheric Cherenkov Telescope (IACT) sensitivities are also shown, as in the following SED plots, as reported in Carmona et al. (2007).

Using a smaller value for the concentration, the number density of particle dark matter pairs decreases, although slightly: for instance, employing  $c_{\text{vir}} = 6$  instead of 10 we get a reduction of less than 10% in the overall normalization factor.

### 3.2 Synchrotron + Inverse Compton models

We also considered Inverse Compton (IC) models, where the hard X-ray emission is due to IC scattering of a population of non-thermal electrons off the cosmic microwave background. We assume that the electron population responsible for the hard X-ray emission has a spectral distribution of the form:

$$\frac{dN_e}{dE_e} = N_0 \left( \frac{E_e}{1 \text{ GeV}} \right)^{-\alpha} \times \exp[-E_e/E_c], \quad (2)$$

i.e. a power-law with index  $\alpha$  plus an exponential cut-off at electron energy equal to  $E_c$ . The election of such a relativistic electron distribution is justified, since radio minihalos can be explained in terms of primary relativistic electrons re-accelerated by magneto-hydrodynamic turbulence (Ferrari et al. 2008). The importance of this mechanism was recently confirmed by Brunetti et al. (2008), who also noticed that spectrum cut-offs are a well-known signature of the turbulence acceleration, implying a corresponding cut-off in the emitting electron population. We note that due to the exponential cut-off in the electron population, there is not an analytical solution that directly links the index  $\alpha$  of the electron population with the observed radio spectral index discussed in section 2.1.4. We set the normalization  $N_0$  to obtain the best possible fit to the *INTEGRAL* hard X-ray data (Eckert et al. 2008). We then compute the integrated gamma-ray flux and the maximal value for the magnetic field compatible at the 95% C.L. along with our upper limits of the diffuse non-thermal radio emission from the core of the Ophiuchus cluster.

The top panel of Fig. 7 shows the parameter space for the cut-off electron energy,  $E_c$ , versus the injected index,  $\alpha$ , of the relativistic electron population, which are the only two free parameters in Equation 2. Shown are also the lines of constant magnetic field. As it is evident from this graphic, very low ( $\lesssim 0.015 \mu\text{G}$ ) values of the magnetic field are excluded by the EGRET data. Similarly, values significantly higher than  $\sim 0.3 \mu\text{G}$  can be mostly excluded because they enter into conflict with the *XMM-Newton* data, or require unreasonable high, or low, values of  $\alpha$ . The preferred values for the average magnetic is in the range from  $\sim 0.02 \mu\text{G}$  up to  $\sim 0.3 \mu\text{G}$ . The bottom panel of Fig. 7 shows the resulting SED for two representative models, which are compatible with the new radio data, the nonthermal X-ray *INTEGRAL* detection and our upper limit to the non-thermal X-ray emission from *XMM-Newton*. The second peak at very high energies ( $\gtrsim 1$  GeV) corresponds to the non-thermal Bremsstrahlung emission. This plot also shows that future high-sensitivity, high-angular resolution radio data, along with sensitive mea-

<sup>2</sup> [http://www-glast.slac.stanford.edu/software/IS/glast\\_lat\\_performance.htm](http://www-glast.slac.stanford.edu/software/IS/glast_lat_performance.htm)

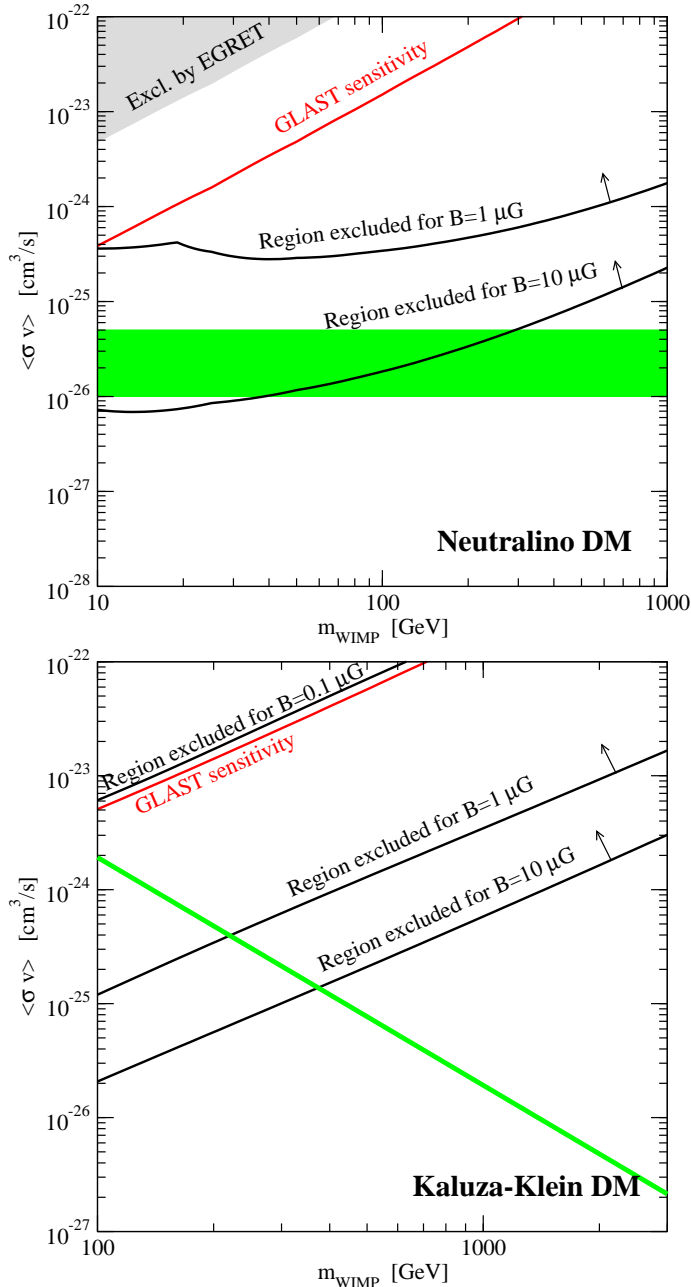


**Figure 5.** The plane of mass and pair-annihilation cross section for neutralino-like dark matter (top) and Kaluza-Klein dark matter (bottom). Regions above the black lines are ruled out by radio data, for the value of the magnetic field indicated on the curves. The Fermi-LAT sensitivity extends down to the red lines, while the gray region is excluded by EGRET. The green regions indicate the preferred portions of the parameter space in the two models.

measurements at high energies will be of much use to further constrain the SED of Ophiuchus within this scenario.

### 3.3 PeV models

Another plausible scenario to account for both the radio and hard X-ray data is that outlined in Inoue, Aharonian & Sugiyama (2005), who find that very high energy pro-

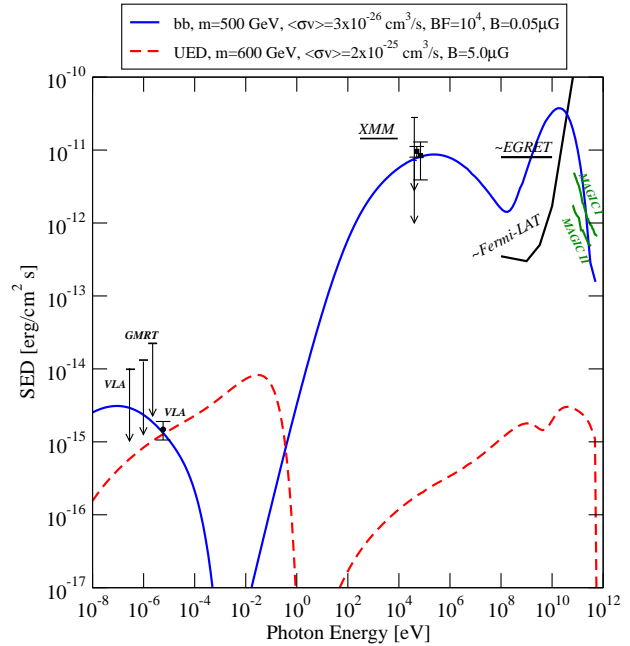


**Figure 6.** The SED for two dark matter models. Note that if the magnetic field is around the  $\mu\text{G}$  level, the limits we obtain are much better than the Fermi-LAT performance, and actually put rather stringent constraints on dark matter models. Only if the average magnetic field is extremely low (solid blue line), then Fermi-LAT measurements will be of very much use for constraining currently proposed models. In this and the following SED plots, the solid points in the X-ray band correspond to the *INTEGRAL* data, while the two arrows in that energy band correspond to the upper limits from Swift/BAT and Suzaku; the XMM and EGRET upper limits are also indicated.

tons resulting from strong accretion shocks produce high energy (TeV-PeV) electron-positron pairs via interactions with the cosmic microwave background, which then radiate synchrotron and inverse Compton emission, peaking respectively at hard X-ray and TeV gamma-ray energies. For simplicity, we modelled the injected electron-positron spectrum as mono-energetic, at an energy specified by the parameter  $E_{\text{inj}}$ . We then computed the equilibrium spectrum by accounting for IC, synchrotron, Bremsstrahlung and Compton energy losses, and neglected spatial diffusion. The resulting electron-positron equilibrium spectrum shows a spectral index  $\alpha \sim 2$  at large energies (between where IC and Synchrotron energy losses dominate,  $E \sim 1$  GeV, and the cutoff energy  $E_c$ ), and a sharp cut-off at  $E_c = E_{\text{inj}}$ . We then fitted for the hard X-ray data and computed the emission at all other frequencies after having re-normalized the electron-positron flux appropriately.

We studied the  $(B, E_{\text{inj}})$  plane (top panel of Fig. 8). The yellow area is excluded by the radio data, while the gray area is ruled out by the EGRET constraints on the gamma-ray emission from the Ophiuchus cluster. We also show in the bottom panel the SED of two models in agreement with the *INTEGRAL* non-thermal detection. Note that both models give comparable synchrotron fluxes (from radio to X-rays), due to a degeneracy of the  $E_{\text{inj}}$  and  $B$  parameters, as it is apparent in the top panel of Fig. 8. The IC peak, instead, depends on the normalization of the electron-positron flux,

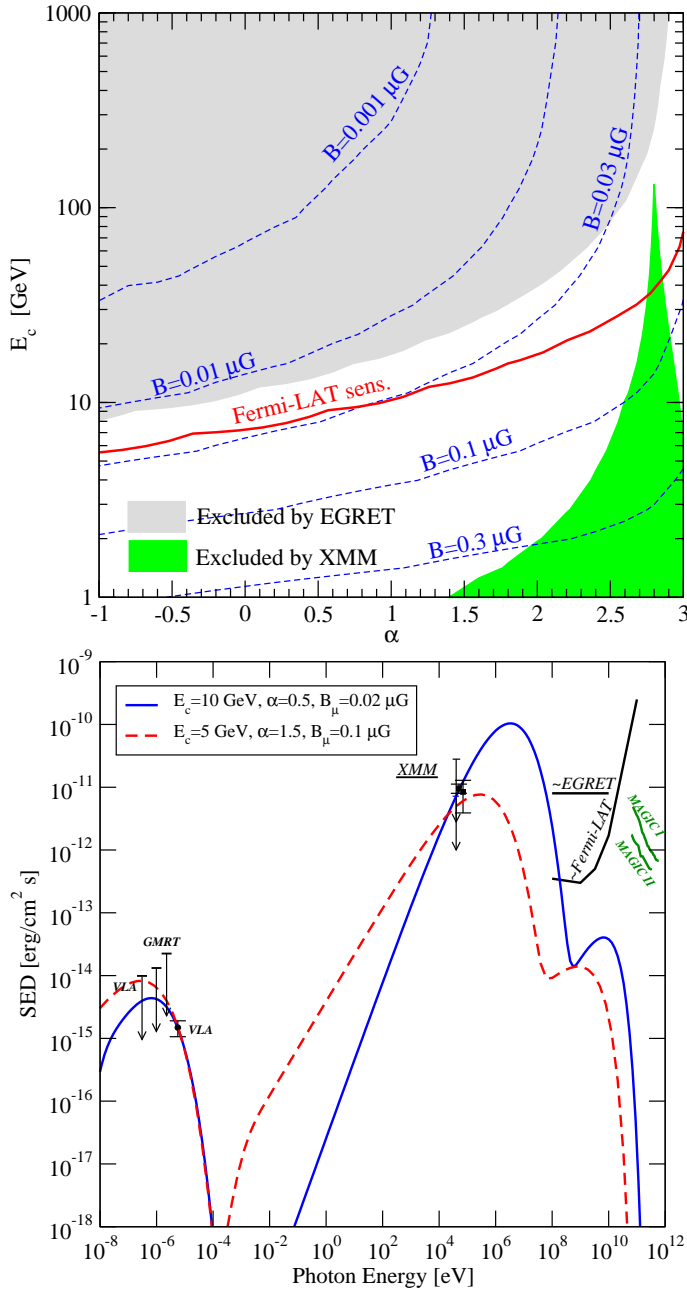


**Figure 7.** Top: The  $(E_c, \alpha)$  plane for models fitting the hard X-ray data. The pairs of  $\alpha, E_c$  excluded by soft X-ray and gamma-ray data are shaded in green and gray, respectively. the Fermi-LAT sensitivity is indicated with a red line. We also show the values of the magnetic field required to have a radio emission compatible with the observations. Bottom: SED for two models compatible with the radio and non-thermal hard-X-ray data. (See main text for details.)

and this in turn depends only on the magnetic field. Therefore, larger magnetic fields imply a suppressed IC emission. As the red dashed model shows, IC models with a soft injection spectral index ( $\alpha \gtrsim 1.5$ ), and that explain both radio and HXR data are generically in tension with the EGRET constraint on the gamma-ray flux. The high energy tail of the synchrotron emission is at a level compatible with the non-thermal hard X-ray data reported by *INTEGRAL*, but

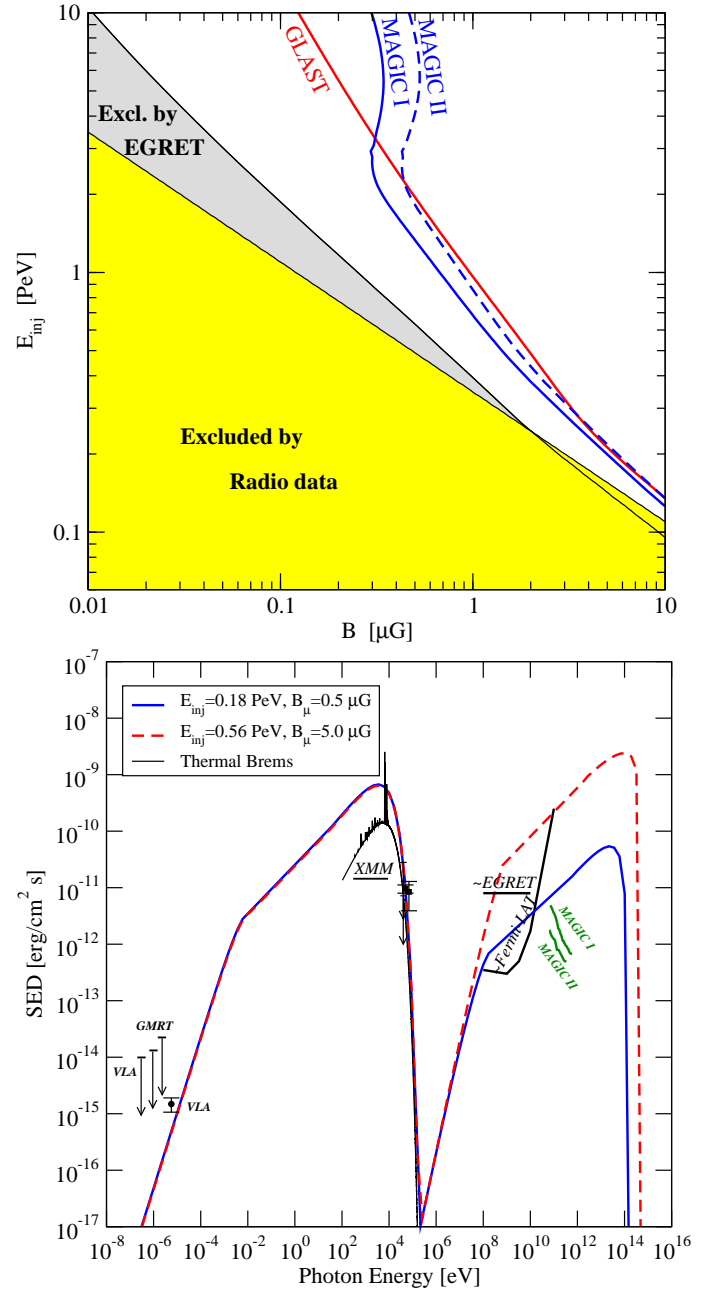


**Figure 8.** Top: The  $(E_{inj}, B)$  plane for PeV models fitting the hard X-ray data. The region shaded in yellow is ruled out by radio data, while the region shaded in gray is ruled out by the EGRET upper limit. Bottom: SED for the two models compatible with the hard X-ray data. Note that the models predict a much larger excess of X-rays with respect to the thermal Bremsstrahlung measured by *INTEGRAL*, which rules them out.

is not compatible with the upper limit to the non-thermal emission in the soft X-ray band that we measured from the *XMM-Newton* data. In addition, the non-thermal soft X-ray emission predicted by the PeV models largely exceeds the thermal Bremsstrahlung measured by *INTEGRAL*, and therefore this family of models can be ruled out.

#### 4 SUMMARY

We present high resolution 240 and 607 MHz GMRT radio observations, complemented with 74 MHz archival VLA radio observations of the Ophiuchus cluster of galaxies, whose mini-radio halo has been recently detected at 1400 MHz. We also present archival *Chandra* and *XMM-Newton* data of the Ophiuchus cluster. Our observations do not show significant radio emission from the mini-halo, hence we present upper limits to the integrated, diffuse non-thermal radio emission of the core of the Ophiuchus cluster.

The *XMM-Newton* observations can be well explained by a two-temperature thermal model with temperatures of  $\simeq 1.8$  keV and  $\simeq 9.0$  keV, respectively. This result is in agreement with previous ones by Fujita et al. (2008), which suggested that the central region of the Ophiuchus cluster is a cooling core. In turn, this result is consistent with the occurrence of a mini-halo, as expected to be found in hot clusters with cool cores, and therefore support the conclusion by Fujita et al. (2008) that Ophiuchus is not the result of a major merger. We also used the *XMM-Newton* data to set up an upper limit to the (non-thermal) X-ray emission from the cluster and therefore constrain the SED of the Ophiuchus cluster.

The high spatial resolution of the radio and X-ray data have allowed us to study separately the diffuse emission of the cluster core from that due to the population of point sources. In particular, we have found a relatively bright radio and X-ray (*Chandra*) point source at the center of the cluster (source A in our images), which is spatially coincident with the *INTEGRAL* hard X-ray source. The flat radio spectrum of this point source and the lack of non-thermal emission has allowed us to associate it to a low-level AGN activity, most likely associated to the cD central galaxy 2MASX J17122774-2322108. This central source is very unlikely to be responsible for the hard X-ray emission detected by *INTEGRAL*, in spite of its apparent spatial coincidence.

Neither our newly obtained radio data at 240 and 607 MHz, nor the archival VLA data at 74 MHz for the Ophiuchus cluster of galaxies detect significant diffuse radio emission from the mini-halo in Ophiuchus, which has been recently at 1400 MHz. The radio and X-ray non-thermal data have dramatic implications for currently proposed scenarios to model the spectral energy distribution (SED) of the Ophiuchus cluster of galaxies. In particular, a synchrotron+IC model is in agreement with the currently available data, if the average magnetic field is between  $\sim 0.02\mu\text{G}$  and  $\sim 0.3\mu\text{G}$ . A pure dark matter scenario can also, in principle, reproduce both radio and X-ray emission, but very large boost factors from dark matter substructures and extremely low values of the average magnetic field are needed. We notice that for a magnetic field value comparable with the expectations from Faraday rotation measures ( $\sim 1\mu\text{G}$ ), GLAST-Fermi and high-resolution radio searches for a diffuse signal from galaxy clusters will have a comparable and complementary reach in the particle dark matter parameter space. Finally, we also explored the possibility of synchrotron and inverse Compton emission arising from PeV electron-positron pairs (via interactions with the CMB), as described in Inoue, Aharonian & Sugiyama (2005). Those models can be ruled out, since they predict a non-thermal soft X-ray emission that largely exceeds the thermal Bremsstrahlung measured by

*INTEGRAL* and the non-thermal X-ray emission inferred from the *XMM-Newton* data.

Given that Ophiuchus is one of the closest galaxy clusters, it can be studied at high resolution and with high sensitivity. Therefore, its study at all wavelengths is encouraged, since it can result in much better constraints of its SED, and will allow for tests on acceleration scenarios, as we have discussed in this paper. In particular, optical spectroscopy is advisable, as it would allow to confirm, or rule out, the membership of some of the sources shown in the radio images presented in this work. Gamma-ray observations would also be very useful to constrain the SED and the particle acceleration mechanisms.

#### ACKNOWLEDGMENTS

We are grateful to the referee for useful comments and suggestions in the paper, and to Jukka Nevalainen for comments, suggestions and helpful advice on the reduction of the *XMM-Newton* data. We also thank Valentí Bosch-Ramon for useful advices. GMRT is run by the National Centre for Radio Astrophysics of the Tata Institute of Fundamental Research. NRAO is a facility of the National Science Foundation operated under cooperative agreement by Associated Universities, Inc. This research has made extensive use of NASA's ADS, and of the NASA/IPAC Extragalactic Database (NED). M.A. Pérez-Torres is a Ramón y Cajal Post Doctoral Research Fellow funded by the Spanish Ministry of Education and Science (MEC) and the Spanish Research Council (CSIC). F. Zandanel acknowledges the support of a JAE PreDoc-CSIC fellowship in the IAA-CSIC, in Granada. M.A. Pérez-Torres, F. Zandanel and F. Prada also acknowledge support by the Spanish MEC through grants AYA 2006-14986-C02-01 and AYA 2005-07789. S. Profumo is partly supported by US Department of Energy Contract DE-FG02-04ER41268 and by NASA Grant Number NNX08AV72G. F. Panessa acknowledges support by ASI I/008/07 grants.

#### REFERENCES

- Ajello M., et al., 2008, arXiv, arXiv:0809.0006
- Atayan A. M., Völk H. J., 2000, ApJ, 535, 45
- Baars J. W. M., Genzel R., Pauliny-Toth I. I. K., Witzel A., 1977, A&A, 61, 99
- Bertone G., Hooper D., Silk J., 2005, PhR, 405, 279
- Blasi P., Gabici S., Brunetti G., 2007, astro, arXiv:astro-ph/0701545
- Brunetti G., et al., 2008, Natur, 455, 944
- Carmona E., et al., 2007, arXiv, arXiv:0709.2959
- Cohen A. S., Lane W. M., Cotton W. D., Kassim N. E., Lazio T. J. W., Perley R. A., Condon J. J., Erickson W. C., 2007, AJ, 134, 1245
- Colafrancesco S., Profumo S., Ullio P., 2006, A&A, 455, 21
- Colafrancesco S., Profumo S., Ullio P., 2007, PhRvD, 75, 023513
- Condon J. J., Cotton W. D., Greisen E. W., Yin Q. F., Perley R. A., Taylor G. B., Broderick J. J., 1998, AJ, 115, 1693
- Dunn R. J. H., Fabian A. C., 2006, MNRAS, 373, 959

- Eckert D., Produit N., Paltani S., Neronov A., Courvoisier T. J.-L., 2008, *A&A*, 479, 27
- Ensslin T. A., Biermann P. L., 1998, *A&A*, 330, 90
- Feretti L., Giovannini G., 2007, *astro*, arXiv:astro-ph/0703494
- Ferrari C., Govoni F., Schindler S., Bykov A. M., Rephaeli Y., 2008, *SSRv*, 134, 93
- Fujita Y., et al., 2008, *PASJ*, 60, 1133
- Govoni F., Murgia M., Markevitch M., Feretti L., Giovannini G., Taylor G. B., Carretti E., 2009, arXiv, arXiv:0901.1941
- Hasegawa T., et al., 2000, *MNRAS*, 316, 326
- Hooper D., Profumo S., 2007, *PhR*, 453, 29
- Inoue S., Aharonian F. A., Sugiyama N., 2005, *ApJ*, 628, L9
- Jeltema T. E., Profumo S., 2008, *ApJ*, 686, 1045
- Johnston M. D., Bradt H. V., Doxsey R. E., Marshall F. E., Schwartz D. A., Margon B., 1981, *ApJ*, 245, 799
- Jungman G., Kamionkowski M., Griest K., 1996, *PhR*, 267, 195
- Molendi S., Gastaldello F., 2008, arXiv, arXiv:0807.2653
- Murgia M., Govoni F., Markevitch M., Feretti L., Giovannini G., Taylor G. B., Carretti E., 2009, arXiv, arXiv:0901.1943
- Navarro J. F., Frenk C. S., White S. D. M., 1996, *ApJ*, 462, 563
- Profumo S., 2008, *PhRvD*, 77, 103510
- Renaud M., Bélanger G., Paul J., Lebrun F., Terrier R., 2006, *A&A*, 453, L5
- Reimer O., Pohl M., Sreekumar P., Mattox J. R., 2003, *ApJ*, 588, 155
- Sanders J. S., Fabian A. C., Allen S. W., Schmidt R. W., 2004, *MNRAS*, 349, 952
- Sanders J. S., Fabian A. C., Dunn R. J. H., 2005, *MNRAS*, 360, 133
- Sarazin C. L., 1999a, *astro*, arXiv:astro-ph/9911439
- Sarazin C. L., 1999b, *ApJ*, 520, 529
- Timokhin A. N., Aharonian F. A., Neronov A. Y., 2004, *A&A*, 417, 391
- Watanabe M., Yamashita K., Furuzawa A., Kunieda H., Tawara Y., 2001, *PASJ*, 53, 605